Egypt. J. Chem. **Vol. 66**, No. 9 pp. 293 - 306 (2023)

Egyptian Journal of Chemistry

http://ejchem.journals.ekb.eg/

ENHANCED PHOTOCATALYTIC DEGRADATION OF METHYLENE BLUE DYE UNDER UV-LIGHT IRRADIATION USING Bi_2S_3/ZnS AND ZnS/ Bi_2S_3 NANOCOMPOSITIES

Ashraf A. El-Bindary[a]*, Mokhtar S. Beheary[b], Noha S. Samra[b], Mina S. Adly[c]

[a]Chemistry Department, Faculty of Science, Damietta University, New Damietta 34517, Egypt.

[b]Environmental Science Department, Faculty of Science, Port Said University, Port Said 42526, Egypt.

[c]Chemistry Department, Faculty of Science, Mansoura University, Mansoura 35511, Egypt.

Abstract

Pure Bi_2S_3, ZnS, and different ratios of Bi_2S_3 to ZnS, and ZnS to Bi_2S_3 have been prepared by hydrothermal method to investigate their efficiency in the adsorption of a toxic cationic methylene blue (MB) dye from synthetic aqueous solutions, and to prove that the heterojunction addition of zinc sulphide to bismuth sulphide and bismuth sulphide to Zinc sulphide with different ratios (1.0, 3.0, 7.0 wt%) significantly improved their photocatalytic activity and methylene blue dye removal. Photodegradation time, initial dye concentrations, and adsorbent doses respectively have been studied. The optimum conditions of methylene blue (MB) dye adsorption were at a contact time of 120 min, 0.05 g/L of pure Bi_2S_3, pure ZnS, 1 wt% Bi_2S_3/ZnS, and 1 wt% ZnS/ Bi_2S_3) in an aqueous solution of pH=7, at room temperature, and the %removal of the dye under these conditions reached about (70%, 60%, 95%, and 91%) respectively, and the dye adsorption kinetic process has been analysed using pseudo-first-order kinetic models. The results presented that the adsorption kinetics of methylene blue (MB) dye followed a pseudo-first-order model very well. FTIR, XRD, XPS, and TEM techniques have been conducted to illustrate the properties and characterizations of the prepared photocatalysts. The noticeable improvement we found in the properties and photodegradation rate of heterostructured photocatalysts compared to single photocatalysts hold considerable promise for the development of the novel as well as for the remediation of the environment.

Keywords: Heterojunction photocatalysts; Hydrothermal; Bi_2S_3; ZnS; methylene blue.

1. Introduction

One of the most significant environmental obstacles to the development of various businesses, particularly the textile industry, is wastewater. Due to the numerous varieties of synthetic dyes employed and the poor fabric absorption of these dyes, enormous amounts of highly colored effluent are discharged into the textile sector [1]. Dyeing is the process of coloring materials with colored compounds that give them their unique tints and make them resistant to washing, light, air, acids, and bases[2]. Industrial dyes are one of the most common types of water pollutants due to their high solubility in water, and before being released into public sewage systems or surface waterways, industrial wastewater must undergo chemical treatment to remove harmful compounds and meet legal limitations[3].

Using processes including adsorption, filtration, sedimentation, ion exchange, and others to remove dyes from wastewater and render them useable while continuing to create new technical systems to remove organic contaminants found in water, such as dyes and heavy metals, from their aqueous solutions [4]. In the last few decades, environmental remediation and water treatment using semiconductor material have drawn remarkable attention. For degradation of environmental pollutants and production of hydrogen[5]. Surface

*Corresponding author e-mail: abindary@du.edu.eg (Ashraf A. El-Bindary)
Received date 21 November 2022; revised date 19 December 2022; accepted date 22 December 2022
DOI: 10.21608/EJCHEM.2022.173941.7212

sensitization, nonmetal, and metal doping are methods that have been explored to enhance photocatalytic activity. Unfortunately, these methods greatly diminish the efficiency of photodegradation due to the high possibility of recombination between photogenerated electrons and dopant holes [6].Another method was investigated to increase the photocatalyst's efficiency inside the visible light range. Mixing a narrow band gap semiconductor with metal and/or other semiconductors creates some unique semiconductor heterojunctions [7]. These semiconductor heterojunctions have demonstrated remarkable efficiency in reducing the rate of photogenerated electron and hole recombination, enhancing thermal stability, and eventually enhancing photocatalytic activity [8]. Recently, there are many important semiconductor heterojunctions have been reported, Metal sulfides, in particular ZnS, have been extensively studied in photocatalysis due to their different catalytic characteristics compared to metal oxides [9]. Under light irradiation, ZnS significantly impacts the photodecomposition of organic contaminants and the production of hydrogen from water [10]. Unfortunately, the use of ZnS as photocatalysts is constrained by three fundamental issues. First, Due to its unusually wide band gap size of 3.66 eV, ZnS can only escape under UV light. The second factor that restricts the conversion of light energy is the photogenerated electron-quick hole's recombination. Third, poor chemical stability could lead to airborne oxidation by oxygen [11]. Therefore, to solve these issues, we must increase the spacing of photogenerated carriers and broaden the reaction range to visible light [12]. Bi_2S_3 is another attractive semiconductor that has drawn attention due to its narrow band gap of 1.3 eV. Bismuth sulfide is a strong light absorber because of its high coefficient of light absorption (approximately 104-105 cm^{-1}) [13]. Due to the high rate of electron-hole pair recombination and the inefficient separation of electron-hole pairs, Bi_2S_3 photocatalytic activity is relatively low [14]. By creating a photo-absorption wavelength red-shift that increases the semiconductor's oxidation-reduction capacity, Bi_2S_3 can act as a coat on another semiconductor, enhancing its capacity to absorb visible light and enhancing the photochemical stability of the semiconductor, enhancing its capacity to absorb visible light and enhancing the photochemical stability of the semiconductorAdditionally, the valence band of Bi_2S_3 is more electronegative than that of ZnS, while the conduction band of Bi_2S_3 has a smaller electropositive than that of similar ZnS [15].

To effectively increase the quantum yield, this study aims to prepare a Bi_2S_3/ZnS heterojunction composite with efficient separation capacity, facilitate the transfer of photogenerated carriers, and restrict the recombination of photogenerated carriers The structural properties and photocatalytic activity of pure ZnS, pure Bi_2S_3, ZnS/Bi_2S_3, andBi_2S_3/ZnS composites must be further discussed and investigated. As a result, ZnS and a semiconductor with a small band gap Bi_2S_3, we design and construct a Bi_2S_3/ZnS composite to further increase the catalytic effectiveness of photocatalytic materials using visible light [16]. Using XRD, TEM, FT-IR, and XPS, the Bi_2S_3/ZnS and Bi_2S_3/ZnS heterojunctions were examined and evaluated. To assess the photocatalytic activity of the samples when exposed to visible light, methylene blue dye was chosen as the pollutant [17].

2. Experimental

2.1. Materials

Bismuth Nitrate $Bi(NO_3)_3.5H_2O$, sodium sulphide (Na_2S), zinc acetate $Zn(CH_3COO)_2.5(H_2O)_2$, ethylene glycol ($HOCH_2CH_2OH$) purchased from ADWIC. The reagents and methylene blue dye were acquired from Sigma Aldrich and utilized directly without purification.

2.2. Preparation of photocatalysts

2.2.1. Preparation of Zinc Sulphide

Pure zinc sulfide is synthesized by dissolving 2.253 g zinc acetate in 20 mL of distilled water. Subsequently, sodium sulfide 0.85 g was dissolved in 20 mL of distilled water, which was gradually added to the initial solution. and allowed to stir for four hours at room temperature. The resulting white precipitate was centrifuged, repeatedly washed with distilled water, and dried at 80 °C [18].

2.2.2. Preparation of Bismuth Sulphide

0.97 g of bismuth nitrate is completely dissolved in 20 mL of distilled water. Furthermore, the solution of sodium sulfide was 0.455 g in 20 mL distilled water, which was added drop by drop and then left for 1 h to stir at 90 °C. Finally, the resulting black precipitate of Bi_2S_3 nanoparticles was centrifuged, multiple times rinsed with distilled water, and then dried for 8 hours at 100 °C [19].

2.2.3. Preparation of Bi_2S_3/ZnS heterostructure

Bi_2S_3/ZnS composite was prepared by hydrothermal method. $(Bi_2S_3)_{1-x}(ZnS)_x$ heterostructure where (X = 1.0, 3.0, 7.0 wt%) were prepared by reaction 2.96 m.mol sodium sulfide, 0.24 m.mol of $Zn(CH_3COO)_2.5(H_2O)_2$ and 1.2 for $Bi(NO_3)_3.5H_2O$ were dissolved in 50 mL of ethylene glycol, then the solution allowed to stir for 1 h at 90 °C. Furthermore, the solution was transferred into a 40 mL Teflon-lined stainless-steel autoclave. Then, the entire mixture was sealed and kept at 130 ˚C for 8 hours. After centrifuging the resulting dark brown solid product, it was collected and properly cleaned with distilled water. Finally, the precipitate overnight dried at 100 °C [20].

2.2.4. Preparation of ZnS/Bi_2S_3 heterostructure

ZnS/Bi_2S_3 composite was prepared by hydrothermal method. $(ZnS)_{1-x}$, $(Bi_2S_3)_x$ heterostructure where (X = 1.0, 3.0, 7.0 wt%), 2.96 mmol sodium sulfide, 0.24 mmol of $Bi(NO_3)_3.5H_2O$ and 1.2 for $Zn(CH_3COO)_2.5(H_2O)_2$ were dissolved in 50 mL of ethylene glycol and agitated for 60 minutes at 90 °C. In addition, the mixture spent 8 hours sealed at 130 ˚C in a stainless-steel autoclave with Teflon lining. After that, a centrifuge was used to separate the dark brown solid result, which was then thoroughly rinsed with distilled water. The precipitate was then dried for 8 hours at 100 ºC [21].

2.2.5. Material characterization

Power XRD PW 150 instrument (Philips) at a high angle employing Cu K irradiation source, with a Ni filter, is used to analyze the crystal structures of all collected samples. The instrument was run at a voltage of 40 kV and a current of 45 mA. A Nicolet 550 FTIR spectrometer was used to measure the IR spectra in the 400–4000 cm1 region. TEM imagesand particle size was collected using a Japanese JEOL-JEM-2100 transition electron microscope that ran at 200 keV. The fine sample powders were suspended in alcohol and then dropped onto a copper grid covered in holey carbon foil to prepare the TEM samples. The grid was then dried at room temperature. Thermo-Fisher Scientific ESCALAB 250 was used to collect X-ray photoelectron spectroscopy (XPS) data to investigate the surface elements and chemical states of materials using a monochromatic Al K source.

2.2.6. Measurement of photocatalytic activity

The photocatalytic activities of the samples were evaluated by monitoring the degradation of methylene blue dye under UV/visible light irradiation. A Hg lamp was purchased from Westinghouse, UAE, and the reaction temperature was kept at 35 °C. The degradation of methylene blue dye with a concentration of 10 mg/L using 0.05 g/L photocatalysts concentration of (Bi_2S_3, ZnS, Bi_2S_3/ZnS, and ZnS/ Bi_2S_3). The suspension was magnetically stirred in the dark for 30 minutes to reach adsorption-desorption equilibrium. At given time intervals through the irradiation, 1.0 mL of the sample was diluted 10 times with distilled water and then centrifuged until complete separation was achieved. On a UV/visible/NIR spectrophotometer (V-570), manufactured by JASCO in Japan the samples were analyzed at the wavelengths (λmax) 664 nm for methylene blue dye.

3. Results and Discussion

3.1. X-ray diffraction

Fig. 1displays the XRD patterns of the Bi_2S_3 and ZnS nanoparticles, as well as the composites of 1 wt% ZnS/Bi_2S_3 and 1 wt% Bi_2S_3/ZnS. The results of the experiment demonstrate that producing too many sulfur ions helps produce Bi_2S_3. Furthermore, the products' distinct peaks demonstrate that the hydrothermal reaction conditions are ideal for good crystallization[22].

As can be seen, the generated ZnS nanoparticles exhibit peaks at 2θ angles at 28.4º, 47.8º, and 56.8°, respectively, which correspond to the (111), (220), and (311) planes.

Three peaks are produced by the cubic of the ZnS phase with the cell parameter. For ZnS nanoparticles. The orthorhombic Bi_2S_3 peaks at (310), (211), (221), (440), and (360) may be precisely indexed to the diffraction peaks at 2θ angles of 25.9°, 28.9°, 31.8°, 45.5°, and 54.7°. However, no contaminant diffraction peaks were seen in these samples, indicating that they were manufactured without impurities [23].

The XRD patterns of ZnS, Bi_2S_3, 1.0% wt. Bi_2S_3/ZnS, and 1.0% wt. ZnS/ Bi_2S_3 composite is displayed.

The XRD patterns of the following materials are shown: ZnS, $Bi_2S_3$1.0% wt. Bi_2S_3/ZnS, and 1.0% wt. ZnS/ Bi_2S_3 composite.

Diffraction peaks at 2θ of 25.9°, 28.9°, 31.8, 45.5°, 47.7°, 54.7°, and 56.5°, which correspond to the indices of the orthorhombic Bi_2S_3 and cubic ZnS planes (111), (211), (220), (221), (311), (360) and (440) [24].

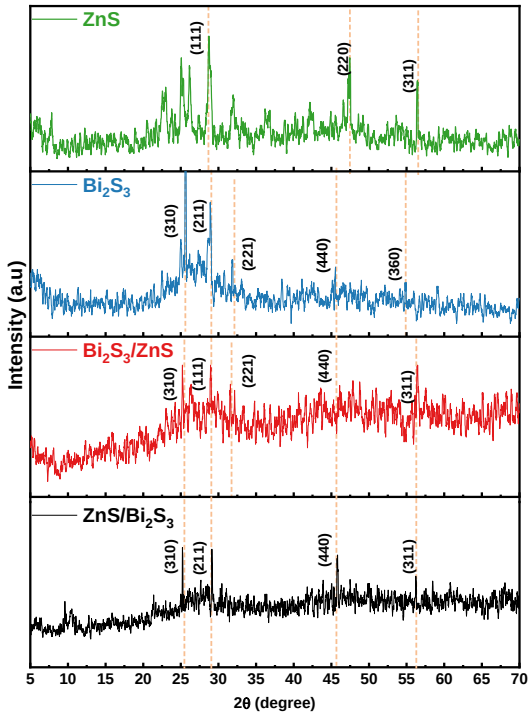

Fig. 1. XRD patterns for ZnS, Bi_2S_3, (1%) Bi_2S_3/ZnS and (1%) ZnS/Bi_2S_3.

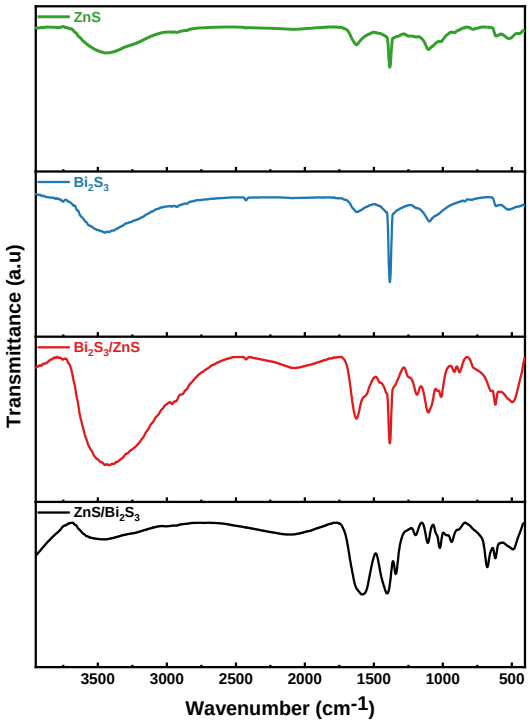

Fig. 2. FTIR spectra of ZnS, Bi_2S_3, (1%)Bi_2S_3/ZnS and (1%)ZnS/Bi_2S_3.

3.2. FTIR analysis

The FTIR spectra of the produced ZnS particles in the frequency range (300-4000 cm^{-1}) are shown in Fig. 2, and they demonstrate IR absorption caused by the various vibrations involved. Bi_2S_3 microsphere, which exhibits different signal peak shapes and locations (25]. The interaction between too much S^{2+} and the Bi_2S_3 during the synthesis process, which caused the peaks to slightly shift, can be seen [26]. According to Fig. 2, the medium intensity stretching vibration appears at 875 cm^{-1}, and 465 cm^{-1} can be assigned to Bi bond vibration. The weak stretching vibration at 634cm^{-1} and 715cm^{-1} is corresponding to C-S bond vibration. Thus the existence of Bi and S can be confirmed $^{-1}$ [27].

3.3. TEM analysis

TEM analysis was used to examine the surface morphologies and particle sizes of prepared samples. (b) Bi_2S_3 exhibits a remarkably uniform Nano rod size (c) distribution with considerable aggregation, a width of roughly 50 nm, and a length between 150 and 200 nm. After the heterojunction process, the typical nanorods structure of Bi_2S_3 was intact, and no significant changes in original morphological appearances were observed [28]. displays the ZnS nanoparticles under a TEM microscope. As demonstrated in the figure, The particle size distribution of ZnS nanoparticles is constrained [29]. According to Fig. 3, which displays a picture of ZnS nanoparticles taken with an HR-TEM, the usual particle size of ZnS nanoparticles is around 40 nm. According to the HR-TEM picture, the d-spacing of the (111) planes correspond to the lattice spacing of 0.312nm. to further corroborate the identification of the Bi_2S_3 nanorods and the production of composites, TEM images of 1 wt% ZnS/Bi_2S_3 and 1 wt% Bi_2S_3/ZnS nanocomposite were collected in Fig. 3 [30]. According to theforegoing findings, the heterojunction not only reduced aggregation of Bi_2S_3 nanorods but also decreased their diameters and provided active sites for dye adsorption on the surface. As a result, it is anticipated that the nanocomposite will exhibit improved photocatalytic properties for the breakdown of contaminants [31].

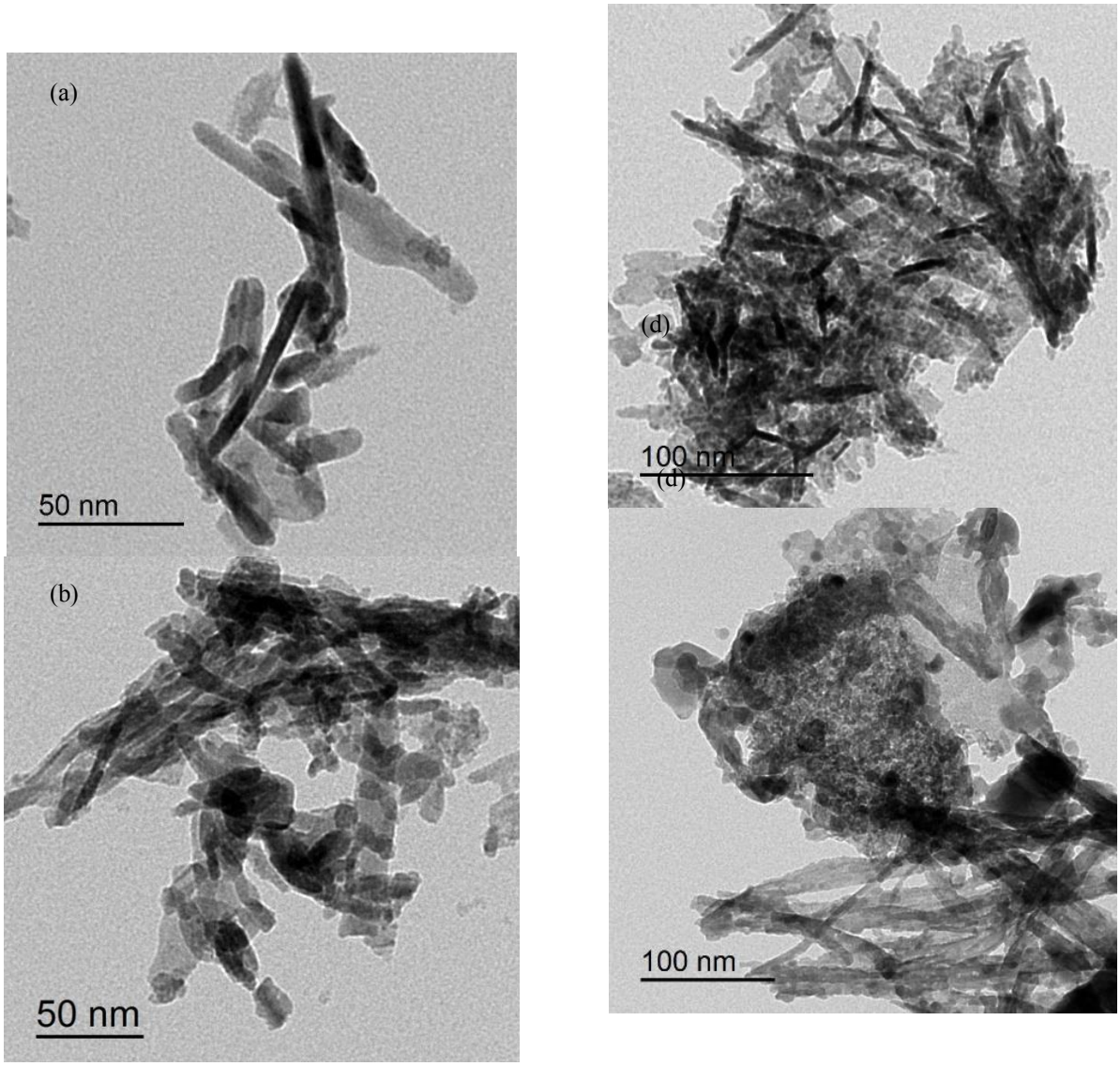

Fig. 3. TEM images of (a) Pure Bi_2S_3, (b, c) 1 wt% ZnS/Bi_2S_3, and (d) 1 wt% Bi_2S_3/ZnS

.

3.4. XPS analysis

X-ray photoelectron spectroscopy (XPS) was used to confirm the formation of (Bi_2S_3, ZnS, Bi_2S_3/ZnS, and ZnS/Bi_2S_3) Fig. 4 shows the results of an XPS survey of ZnS nanoparticles. Because of spin-orbit coupling, ZnS is responsible for splitting Zn 2p electron levels are separated into Zn $2p_{3/2}$ (1023.0 eV) and Zn $2p_{1/2}$ (1046.0 eV) components Sulfur that exists as sulfides is represented by a single peak at 162.2 eV binding energy value in the S 2pelectron level spectra of the ZnS sample depicted in Fig. 4 [32]. Furthermore, the primary components of bismuth sulfide, Bi and S, were also detected in the survey XPS spectrum, supporting the production of Bi_2S_3 nanorods (Fig. 4). Characteristic two prominent peaks at 158.1 eV and 163.4 eV with 5.3 spacing are found in the high-resolution XPS of the Bi 4f area, and they are Bi $4f_{7/2}$ and Bi $4f_{5/2}$, respectively, inconsistent with the typical Bi^{3+} valance state in Bi_2S_3. Additionally, the two peaks at 162.0 and 160.9 eV found between Bi $4f_{7/2}$ and Bi $4f_{5/2}$ were assigned to S $2p_{1/2}$ and S $2p_{3/2}$, respectively [33].

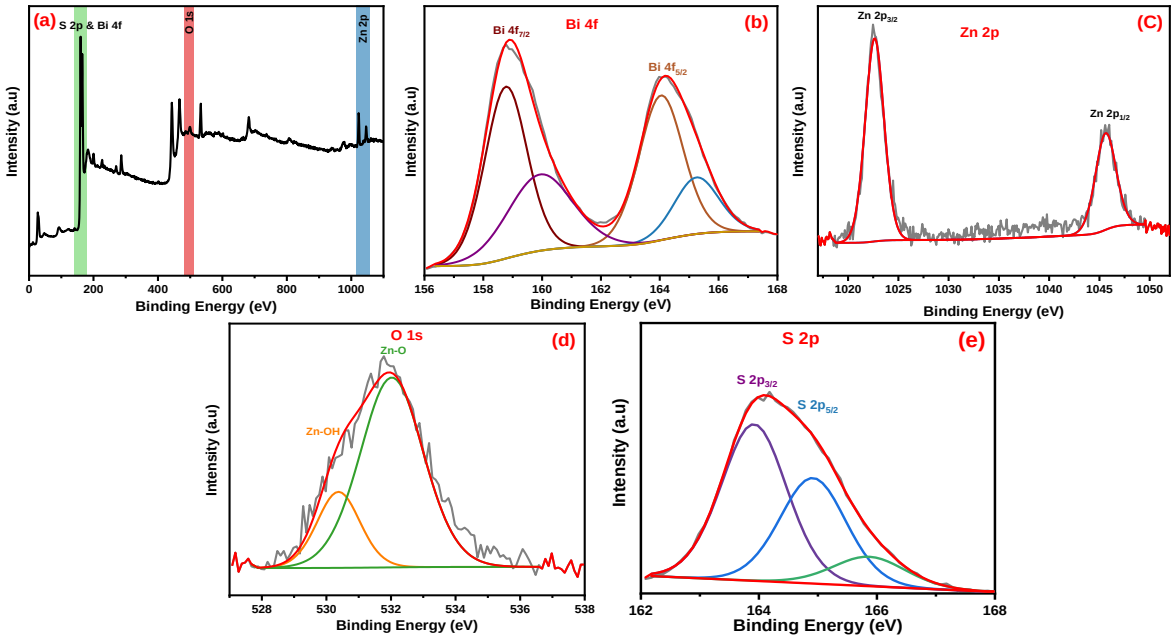

Fig. 4. (a) XPS of (1%)ZnS/Bi_2S_3composite, (b) HR-XPS of Bi 4f, (c) HR-XPS of Zn 2p, (d) HR-XPS of O 1s and (e) HR-XPS of S 2p.

3.5. Photocatalytic degradation of methylene blue dye

3.5.1. Effect of photodegradation time

When exposed to UV-visible radiation, methylene blue dye is photo catalytically degraded in the case of pure and ZnS and pure Bi_2S_3 resulting in nearly 60% and 70%, respectively. In the case of the degradation of methylene blue dye, the addition of ZnS to Bi_2S_3 enhances the degradation percentage [34].

ZnS was added by different percentages (1.0, 3.0, and 7.0 wt%), where the optimum sample was 1 wt% ZnS/Bi_2S_3 with 91% degradation (Fig. 5a). Furthermore, the degradation of methylene blue dye was enhanced by the incorporation of Bi_2S_3 to the structure of ZnS. The degradation activity reached the maximum at 1 wt% Bi_2S_3/ZnS as illustrated in Fig. 5b. The degradation performance increased to 95% and then decreased by increasing the dopant, This could be caused by obstructing the active sites on the photocatalyst surface [35].

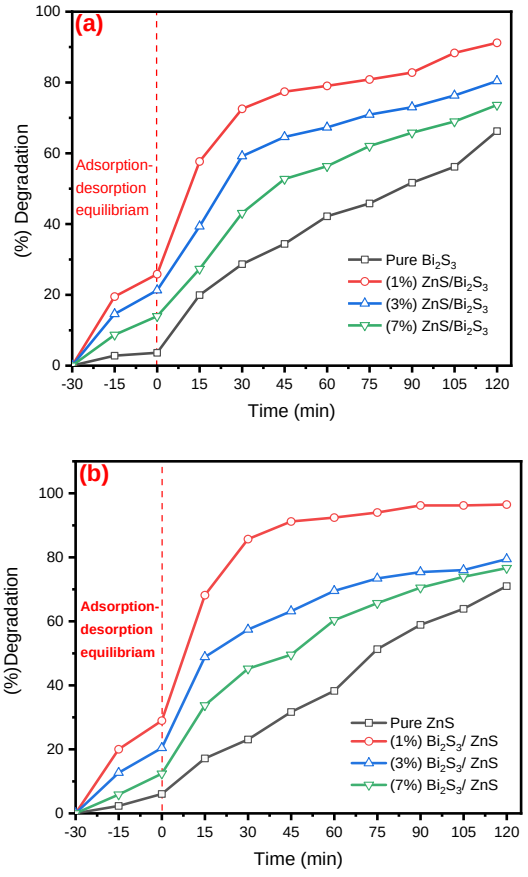

Fig. 5. (a) photocatalytic activity of Bi_2S_3 compared with the photocatalytic activity of 1.0, 3.0, 7.0 wt% of

ZnS/Bi_2S_3 and (b) photocatalytic activity of ZnS compared with the photocatalytic activity of 1.0, 3.0, 7.0 wt% of Bi_2S_3/ZnS on methylene blue dye. (Conditions: dye concentration = 10 mg/L, pH = 7 and catalyst dose = 100 mg/L at room temperature).

3.5.2. Effect of dye concentration

With various dye concentrations, an experiment was undertaken, i.e., 5, 10, 20, 30, and 50 mg/L with 50 mg of 1 wt% ZnS/Bi_2S_3 and 1 wt% Bi_2S_3/ZnS photocatalysts for degradation of methylene blue dye, According to Fig. 6, the photocatalytic degradation efficiency dropped as the original dye concentration increased because less light was being absorbed by the photocatalyst. A solution with a high dye concentration makes it harder for light to penetrate [36]. The photocatalytic degradation mechanism may be impacted by the number of organic contaminants, such as dyes. At low concentrations, the typical mechanism for deterioration involves both the photoinduced electron and hole [37]. The degradation mechanism is dependent on the photocatalyst's contact angle and when compared to the preceding mechanism, the radical concentration is not as high, leaving a significant amount of dye behind. This is because high concentrations of the pollutant or dye molecules block the active centers on the catalyst surface, and the radical concentration is lower than it was in the previous mechanism [38].

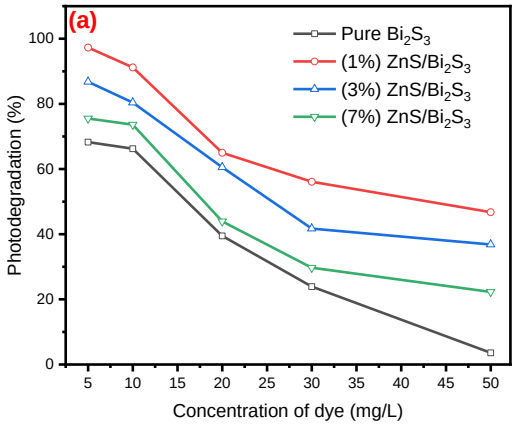

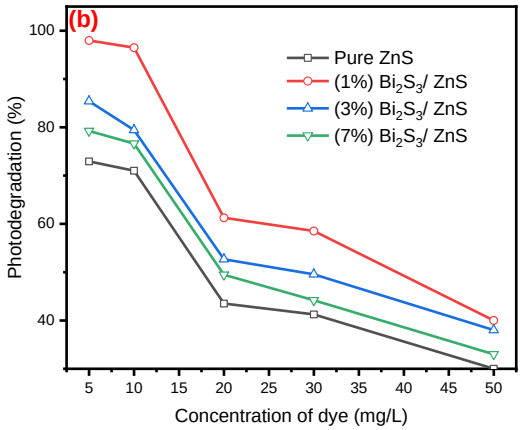

Fig. 6. Photocatalytic degradation at different concentrations of methylene blue dye (a) Bi_2S_3 compared with 1.0, 3.0, 7.0 wt% of ZnS/Bi_2S_3 and (b) ZnS compared with 1.0, 3.0, 7.0 wt% of Bi_2S_3/ZnS. (Conditions: dye concentration = 5, 10, 20, 30, and 50 mg/L, volume = 100 mL, pH = 7, and catalyst dose = 50 mg at room temperature).

3.5.3. Effect of catalyst dose

One of the major factors impacting the kinetics of photocatalytic degradation is the concentration of the catalyst. The photocatalyst was used in an experiment at dosages of 0.015, 0.025, 0.050, 0.075, and 0.1 g/L. As seen in Fig. 7, the photocatalytic degradation of dyes increased as photocatalyst concentration increased. Additionally, the number of photons adsorbed on active sites rose with the concentration of photocatalyst, and the quantity of adsorbed dye molecules increased as well [39].

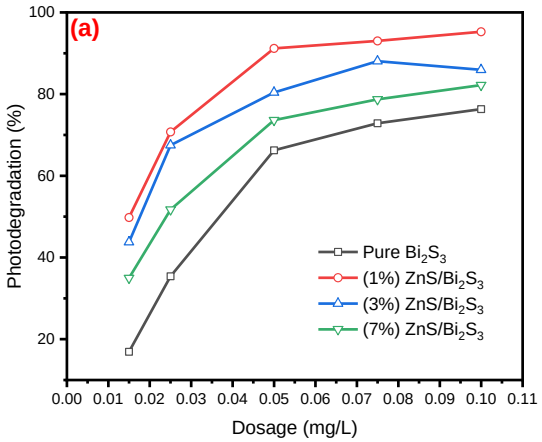

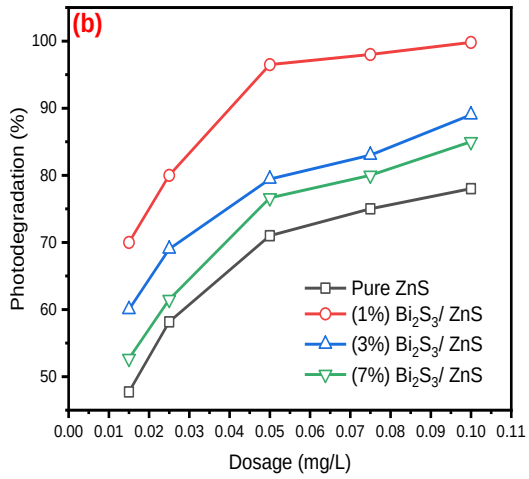

Fig. 7. Photocatalytic degradation at different catalyst doses of methylene blue dye using:(a)Bi_2S_3 compared with 1.0, 3.0, 7.0 wt% of ZnS/Bi_2S_3 and (b) ZnS compared with 1.0, 3.0, 7.0 wt% of Bi_2S_3/ZnS. [Conditions: dye concentration = 10 mg/L and volume = 100 mL and pH = 7 at room temperature].

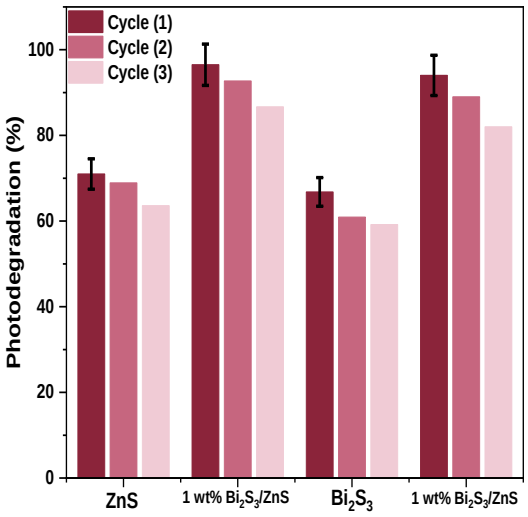

Fig. 8. Photodegradation percentage of ZnS, (1%)Bi_2S_3/ZnS, Bi_2S_3 and (1%)ZnS/Bi_2S_3 over three cycles of reusability.

3.6. Stability and reusability of photocatalyst

the upkeep of high photocatalytic activity and the recyclable nature of the photocatalysts are the two parameters that are most crucial for practical applications. Hence, to investigate the stability of ZnS, Bi_2S_3, 1 wt% ZnS/Bi_2S_3, and 1 wt% Bi_2S_3/ZnS photocatalysts, we conducted tests on the photocatalytic breakdown of methylene blue dye in the presence of UV light. The photocatalyst was centrifuged apart and cleaned with distilled water and ethanol after each experiment [41).

The samples were then reused for other studies after dehydrating in a 100 °C oven. As can be shown, the efficiency of methylene blue dye degradation after 120 min decreased from 70.99% to 63.34%, 66.8% to 59.17%, 94.96% to 82.65%, and 96.5% to 86.66% after three cycles for ZnS, 1 wt% Bi_2S_3/ZnS, Bi_2S_3 and 1 wt% ZnS/Bi_2S_3 respectively as shown in Fig. 8. Because it is impossible to prevent photocatalyst loss during cycle processes, the samples' photocatalytic activity was slightly decreased. The photocatalysts have a high photocatalytic activity as a result, and they are durable under UV radiation [42].

3.7. Degradation kinetics

To measure the impact of different alterations on the photocatalytic activity of ZnS, Bi_2S_3, 1 wt% Bi_2S_3/ZnS, and 1 wt% ZnS/Bi_2S_3, the first-order reaction kinetic equation $\ln(C_t/C_0) = -kt$ was used to fit the kinetics of methylene blue dye degradation (where C_t and C_0 represent the methylene blue dye concentrations at the start of the experiment and during it, respectively; k represents the reaction rate constant, and t represents the reaction time) [43].

Different photocatalysts degrade methylene blue dye in a pseudo-first-order kinetics manner with a correlation coefficient. (R^2= 0.99045, 0.99345, 0.96922, and 0.97936) for ZnS, Bi_2S_3, 1 wt% Bi_2S_3/ZnS and 1 wt% ZnS/Bi_2S_3, respectively[44].
The first-order equation kinetics that characterizes the photocatalytic degradation of methylene blue dye is indicated by the slope of the first-order linear plot, as shown in Fig. 9. The apparent rate constants for the degradation process are estimated graphically and are found to be, -0.00298, -0.01143 and -0.00292 min^{-1} for pure ZnS, Bi_2S_3, 1 wt% Bi_2S_3/ZnS and 1 wt% ZnS/Bi_2S_3respectively [45].

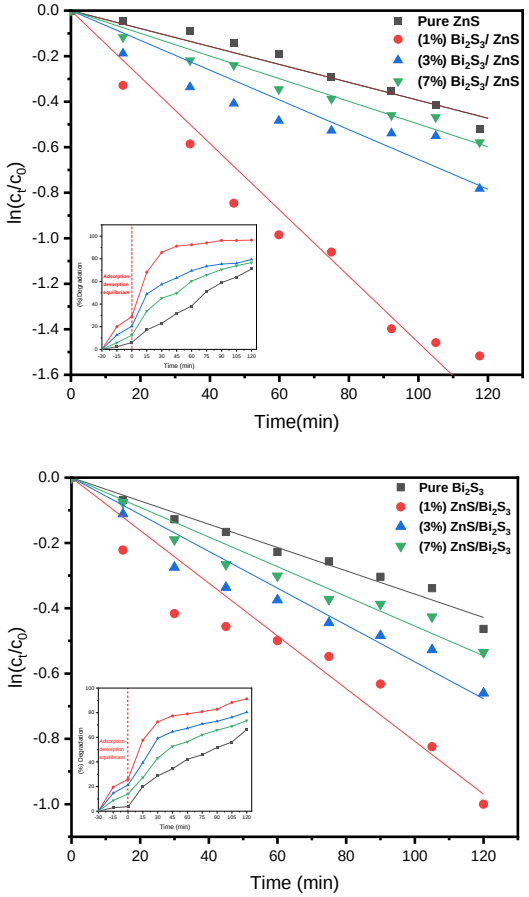

Fig. 9. Photocatalytic degradation kinetic curves of methylene blue dye over (a) Bi_2S_3, 1 wt% ZnS/Bi_2S_3 and (b) ZnS, 1 wt% Bi_2S_3/ZnS in comparison with the photocatalytic activity of photocatalysts (100 mg/L dye concentration, 0.05 g/Ldosage, and pH = 7) under UV irradiation.

3.8. Photocatalytic mechanism

Reactive radical capture tests were carried out to identify the primary active elements in the photocatalytic degradation of methylene blue dye and investigate its photocatalytic process. Electron-hole recombination events were triggered when photons with energies larger than the semiconductor bandgap illuminated the photocatalyst [46]. Then, on the photocatalyst surface, photoactive centers were produced and electron-hole pairs were separated [47].

During the irradiation of the photocatalyst, these photoactive centers created the reactive species e^-, h^+, $^{\bullet}OH^-$, and $^{\bullet}O_2^-$ leading to redox reactions that degraded the dyes. Uncertainty persists over the role of valence band holes and conduction band electrons in the photocatalytic process. understanding the mechanism of ZnS, Bi_2S_3, 1 wt% Bi_2S_3/ZnS, and 1 wt% ZnS/Bi_2S_3 in the methylene blue dye degradation hinges on determining which reactive compounds have the greatest impact [48]. The photocatalytic reaction on the degradation of methylene blue dye over Bi_2S_3 photocatalyst requires the separation of photoelectrons and holes as well as the absorption of light by the samples; the potential photodegradation mechanism of Bi_2S_3 is depicted in Fig. 10 (a). Bi_2S_3 microsphere's 1.3 eV narrow band gap allows it to absorb visible light [49]. Bi_2S_3 is easily inspired to produce photon-generated carriers under visible radiation. And generated electrons from the valence band of the Bi_2S_3 photocatalyst are then easily transported to the suitable power conduction band, leaving a lot of holes there [50]. Even better, the architectures of the samples can successfully stop photoelectrons and holes from recombining, increasing photocatalytic activity. Hydroxyl radical production may be aided by gaps in the photocatalyst's valence band generated by $^{\bullet}OH$ groups absorbed on the surface. In addition, the absorbed molecular oxygen (O_2) eliminates the electrons to produce $^{\bullet}O_2^-$ radicals [51]. The radical ions $^{\bullet}OH$ and $^{\bullet}O_2^-$ will cause the decomposition of methylene blue dye. The following equations could be considered the main reaction steps for the photodegradation of methylene blue dye under visible-light irradiation [52].

in the reaction solution of Bi_2S_3 photocatalyst as shown in Fig. 10 (a). While adding potassium iodide somewhat reduced the photocatalytic degradation of methylene blue dye, adding silver nitrate increased the photocatalytic activity up to 90%. However, the removal rate is significantly decreased by the addition of a scavenger for $^{\bullet}OH$ (isopropanol) and $^{\bullet}O_2^-$ to 35% and 21%, respectively (benzoquinone). The $^{\bullet}OH$ and $^{\bullet}O_2^-$ shown in Eqs. (1-8) are the main reactive species during the photocatalytic breakdown of methylene blue dye by Bi_2S_3[53].

The photodegradation of methylene blue dye over ZnS was studied using silver nitrate as an (e^- scavenger), potassium iodide as an (h^+ scavenger), benzoquinone as an ($^{\bullet}O_2^-$ scavenger)and isopropanol as an ($^{\bullet}OH$ scavenger) in the reaction solution of ZnS photocatalyst. Adding silver nitrate improved the photocatalytic activity of ZnS while the photocatalytic degradation of methylene blue dye has been partially slowed down by the addition of potassium iodide. The removal rate, however, has significantly decreased to 45% and 29%. The addition of a scavenger for $^{\bullet}OH$ (isopropanol) and $^{\bullet}O_2^-$ (benzoquinone). As can be seen, the removal rate drops when scavengers are present, as shown by the following pattern: benzoquinone > isopropanol

>potassium iodide > silver nitrate as shown in Fig. 10 (b) [54].

Therefore, the $^{\bullet}OH$ and $^{\bullet}O_2^-$ are the major reactive species during the photocatalytic breakdown of methylene blue dye. When ZnS was exposed to UV radiation, powerful photons caused electron-hole pairs to form. The holes were concentrated by dissolved H_2O to make $^{\bullet}OH$ radiation, while the electrons typically reacted with oxygen to produce superoxide radiation ($^{\bullet}O_2^-$) following Eqs. (1-8)[55]. Bi_2S_3 is one of the many semiconductors that can produce photoelectrons and holes when activated by visible light (light with a wavelength greater than ($\lambda >$ 420 nm). The reconstructed conduction band edge potential of Bi_2S_3 is therefore greater than that of ZnS in the ZnS/Bi_2S_3 composite (leaving holes on the Bi_2S_3 valence band) [56]. It is simple to transfer the photogenerated holes on the ZnS valence band to the Bi_2S_3 valence band. The oxygen peroxide radicals $^{\bullet}O_2^-$ with significant oxidizing capabilities might be produced by the photogenerated electrons from Bi_2S_3. Therefore, $^{\bullet}OH$ might be produced directly from the photogenerated holes in Bi_2S_3. (Eqs. 1-8) provide the key reactions.

Herein, the effects of different scavengers of methylene blue dye photodegradation have been explored. silver nitrate (e^- scavenger), potassium iodide (h^+ scavenger), benzoquinone ($^{\bullet}O_2^-$ scavenger), and isopropanol ($^{\bullet}OH$ scavenger) were added to the reaction solution containing 1 wt% ZnS/Bi_2S_3 composite. The findings revealed that 13.8% of methylene blue dye could be broken down by isopropanol, proving that hydroxyl radicals have a big impact on photodegradation. On the other hand, in the reaction systems including KI and benzoquinone, respectively, 69.7% and 75.3% of methylene blue dye were photodegraded. These findings suggested that hydroxyl radicals might encourage methylene blue dye photodegradation as shown in Fig. 10 (c).

$$\text{photocatalyst} + h\nu \rightarrow \text{photocatalyst}\,(h^+) + \text{photocatalyst}\,(e^-) \quad (1)$$

$$H_2O \rightarrow H^+ + OH^- \quad (2)$$

$$e^- + O_2 \rightarrow {}^{\bullet}O_2^- \quad (3)$$

$$^{\bullet}O_2^- + H^+ \rightarrow {}^{\bullet}HO_2 \quad (4)$$

$$^{\bullet}HO_2 + H^+ + e^- \rightarrow H_2O_2 \quad (5)$$

$$H_2O_2 + e^- \rightarrow OH^- + {}^{\bullet}OH \quad (6)$$

$$h^+ + OH^- \rightarrow {}^{\bullet}OH \quad (7)$$

$$^{\bullet}OH \text{ or } {}^{\bullet}O_2^- + \text{Organic pollutants} \rightarrow \text{products} \rightarrow CO_2 + H_2O \quad (8)$$

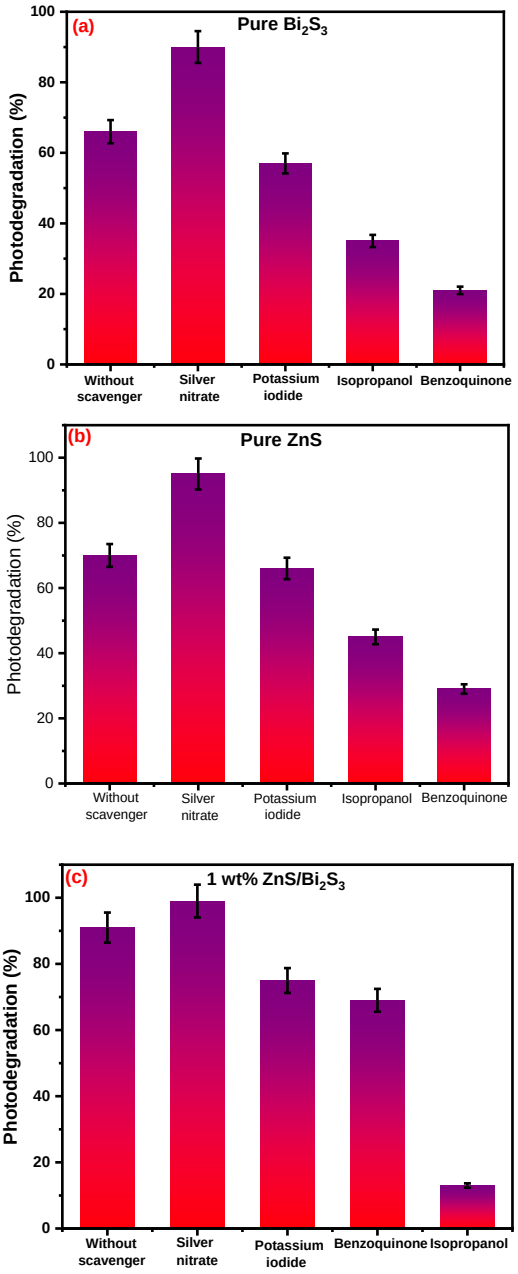

Fig. 10. Degradation ratio of methylene blue dye over (a) Bi_2S_3, (b) ZnS, and (c) 1 wt% ZnS/Bi_2S_3 in the absence and presence of 5.0 %wt. various scavengers (potassium iodide, isopropanol, benzoquinone, and silver nitrate) under UV irradiation for 30 min (30 mg/L dye concentration, 0.6 g/L photocatalyst dosage, and pH = 7).

In Bi_2S_3/ZnS composites, For the division and transmission of charge carriers is favorable [57]. When exposed to visible light, both ZnS andBi_2S_3 are readily excited, and the accompanying photogenerated electrons and holes are produced (Eq.

9). The two semiconductors are nearby, allowing photogenerated electrons to move from the ZnS conduction band to the Bi_2S_3 conduction band effectively. The photogenerated electrons may interact with the system's already-present electron acceptors, like O_2, and reduce them to an anion called superoxide radical $^{\bullet}O_2^-$ (Eq. 10) Under the influence of the band energy potential difference, photogenerated holes in the ZnS valence band can simultaneously migrate to the Bi_2S_3 valence band [58]. One way that the photogenerated holes can function is as a direct oxidant (Eq. 11), Nonetheless, the photogenerated holes can react with the system's existing OH/H_2O to produce the hydroxyl free radical $^{\bullet}OH$ (Eq. 12) [59]. By oxidizing the photo-generated hole, the decomposition of methylene blue dye can be completed, the photo-induced Effective separation of electrons and holes is possible, and electron-hole pair recombination can be regulated (Eq. 11), superoxide radical anion $^{\bullet}O_2^-$ (Eq. 13) and hydroxyl free radical $^{\bullet}OH$ (Eq. 14) directly[60].

$$Bi_2S_3/ZnS + hv \rightarrow Bi_2S_3/ZnS\ (h^+) + (e^-) \quad (9)$$

$$O_2 + (e^-) \rightarrow {}^{\bullet}O_2^- \quad (10)$$

$$(h^+) + \text{organic pollutant} \rightarrow \text{Products} \quad (11)$$

$$(h^+) + H_2O \rightarrow {}^{\bullet}OH + H^+ \quad (12)$$

$$^{\bullet}O_2^- + \text{organic pollutants} \rightarrow \text{Products} \quad (13)$$

$$^{\bullet}OH + \text{organic pollutant} \rightarrow \text{Products} \quad (14)$$

Fig. 11 depicts the degradation effect of methylene blue dye over 1 wt% Bi_2S_3/ZnS composite with various scavengers. Without any scavengers, the breakdown rate of methylene blue dye after 30 minutes of illumination is 96.1%. The degradation ratio of methylene blue dye reduces noticeably when benzoquinone is added as a superoxide radical scavenger, demonstrating the significance of superoxide radical anion $^{\bullet}O_2^-$ in the photocatalytic activity The degradation ratio decreases noticeably when isopropanol is added as a hydroxyl free radical scavenger of $^{\bullet}OH$, demonstrating that this radical is also a significant oxidant in the photocatalytic degradation process The degradation ratio decreases noticeably when isopropanol is added as a hydroxyl free radical scavenger of $^{\bullet}OH$, demonstrating that this radical is also a significant oxidant in the photocatalytic degradation process. According to Fig. 11, adding potassium iodide to the mixture significantly inhibits the degradation of methylene blue dye, indicating that photogenerated hole h^+ is crucial to the success of the photocatalytic degradation process. It may be inferred from the data above that h^+ is primarily responsible for the degradation of methylene blue dye. Meanwhile, the photocatalytic breakdown process is also accelerated by $^{\bullet}O_2^-$ and $^{\bullet}OH$.

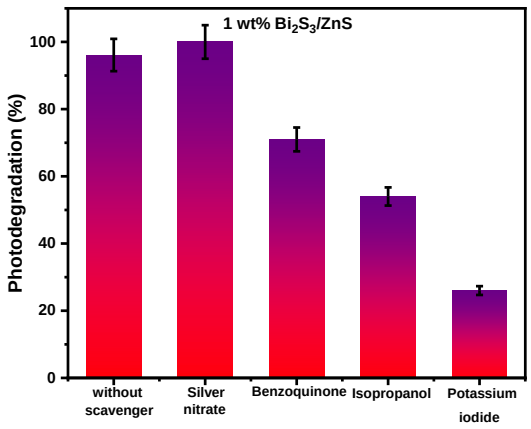

Fig. 11. Degradation ratio of methylene blue dye over 1 wt% Bi_2S_3 / ZnS in the absence and presence of 5.0 %wt. of various scavengers (potassium iodide, isopropanol, benzoquinone, and silver nitrate) under UV irradiation for 30 min (30 mg/L dye concentration, 0.6 g/L dosages, and pH = 7).

4. Conclusions

The conclusions section should come in this section at the end of the article, before the acknowledgements. The ZnS, Bi2S3, $(Bi_2S_3)_x(ZnS)_{1-x}$ and $(ZnS)_x(Bi_2S_3)_{1-x}$ (x = 1.0, 3.0, 7.0 wt%) Composites were created using a hydrothermal process. The samples were analyzed using XRD, FTIR, TEM, and XPS. Results show that ZnS cubic and Bi_2S_3 orthorhombic phases are both present, leading to the creation of composites. By combining the two materials, Bi_2S_3/ZnS and ZnS/Bi_2S_3 composites' absorption and transmittance can be improved up to 91% and 95%, respectively. We get to the conclusion that the composites exhibit strong visible light responsiveness, strong methylene blue dye adsorption capacity, and strong photocatalytic activity. The kinetics were also studied, which agreed with a pseudo-first-order very well.

5. Conflicts of interest

There are no conflicts to declare.

6. Acknowledgments

The authors would like to express their gratitude to Surface and Catalysis Lab, Mansoura University.

7. References

[1] Adly MS, El-Dafrawy SM, El-Hakam SA. Application of nanostructured graphene oxide/titanium dioxide composites for photocatalytic degradation of rhodamine B and acid green 25 dyes. Journal of Materials Research and Technology. 2019;8(6):5610-22.

[2] El-Bindary AA, El-Marsafy SM, El-Maddah AA. Enhancement of the photocatalytic activity of ZnO nanoparticles by silver doping for the degradation of AY99 contaminants. Journal of Molecular Structure. 2019;1191:76-84.

[3] El-Dossoki FI, Atwee TM, Hamada AM, El-Bindary AA. Photocatalytic degradation of Remazol Red B and Rhodamine B dyes using TiO2 nanomaterial: estimation of the effective operating parameters. Desalination and Water Treatment. 2021;233:319-30.

[4] El-Katori EE, Ahmed MA, El-Bindary AA, Oraby AM. Impact of CdS/SnO2 heterostructured nanoparticle as visible light active photocatalyst for the removal methylene blue dye. Journal of Photochemistry and Photobiology A: Chemistry. 2020;392.

[5] Faisal M, Rashed MA, Ahmed J, Alsaiari M, Alkorbi AS, Jalalah M, et al. Rapid photodegradation of linezolid antibiotic and methylene blue dye over Pt nanoparticles/polypyrrole-carbon black/ZnO novel visible light photocatalyst. Journal of Environmental Chemical Engineering. 2021;9(6).

[6] El-Apasery MA, Aly AA, Ahmed DA. Decolorization of Reactive Dyes, Part V: Eco-Friendly Approach of Reactive Red 195 Dye Effluents Decolorization Using Geopolymer Cement Based on Metakaolin %J Egyptian Journal of Chemistry. 2022;65(12):129-35.

[7] Alaraby R, El Sayed MM. Methylene Blue Cationic Dye Removal using AA-Am Hydrogel as An Efficient Adsorbent %J Egyptian Journal of Chemistry. 2022;65(12):1-10.

[8] Almhana NM, Al- Najjar SZ, Naser ZA, Al-Sharify ZT, Nail TH. Photocatalytic Degradation of Textile Dye from Wastewater by using ZnS/TiO2 Nanocomposites Material %J Egyptian Journal of Chemistry. 2022;65(13):481-8.

[9] Benattou H, Benramdane N, Berouaken M. Thin film bismuth(III) sulfide/zinc sulfide composites deposited by spray pyrolysis. Results in Physics. 2017;7:3847-52.

[10] Bhavsar KS, Labhane PK, Murade VD, Dhake RB, Sonawane GH. A photocatalyst: Zinc sulfides nanospheres immobilized on activated carbon for the abatement of aquatic organic pollutants. Inorganic Chemistry Communications. 2021;133.

[11] Boosagulla D, Mandati S, Allikayala R, Sarada BV. Growth mechanism of pulse electrodeposited cadmium sulfide and zinc sulfide thin films with tartaric acid and glycerol as additives. Thin Solid Films. 2022;741.

[12] Caglar B, Guner EK, Ersoy S, Caglar S, Özdemir AO, Özdokur KV, et al. Bi2S3 nanorods decorated on bentonite nanocomposite for enhanced visible-light-driven photocatalytic performance towards degradation of organic dyes. Journal of Alloys and Compounds. 2021;885.

[13] Cai J, Liu D, Shen P, Zhang X, Song K, Jia X, et al. Effects of heating-sulfidation on the formation of zinc sulfide species on smithsonite surfaces and its response to flotation. Minerals Engineering. 2021;169.

[14] Fathy N, Elkhouly S, Aboelenin R. Carbon xerogel/Carbon Nanotubes Nanohybrid Doped with Ti for Removal of Methylene Blue Dye. Egyptian Journal of Chemistry. 2019;0(0):0-.

[15] Azzam E, Fathy N, El-Khouly S, Sami R. Enhancement the photocatalytic degradation of methylene blue dye using fabricated CNTs/TiO2/AgNPs/Surfactant nanocomposites. Journal of Water Process Engineering. 2019;28:311-21.

[16] Kiwaan HA, Atwee TM, Azab EA, El-Bindary AA. Efficient photocatalytic degradation of Acid Red 57 using synthesized ZnO nanowires. 2019;66(1):89-98.

[17] Cao Y, El-Shorbagy MA, Sharma K, Alamri S, Rajhi AA, Anqi AE, et al. In-situ synthesis of a novel ZnO/CuCo2S4 p-n heterojunction photocatalyst with improved phenol and rhodamine B degradation performance and investigating the mechanism of charge carrier separation. Journal of Photochemistry and Photobiology A: Chemistry. 2022;425.

[18] Kiwaan HA, Atwee TM, Azab EA, El-Bindary AA. Photocatalytic degradation of organic dyes in the presence of nanostructured titanium dioxide. Journal of Molecular Structure. 2020;1200.

[19] Chankhanittha T, Komchoo N, Senasu T, Piriyanon J, Youngme S, Hemavibool K, et al. Silver decorated ZnO photocatalyst for effective removal of reactive red azo dye and ofloxacin antibiotic under solar light irradiation. Colloids and Surfaces A: Physicochemical and Engineering Aspects. 2021;626.

[20] Chen L, Xu P, Wang H. Photocatalytic membrane reactors for produced water treatment and reuse: Fundamentals, affecting factors, rational design, and evaluation metrics. J Hazard Mater. 2022;424(Pt B):127493.

[21] Jindal H, Kumar D, Sillanpaa M, Nemiwal M. Current progress in polymeric graphitic carbon nitride-based photocatalysts for dye degradation. Inorganic Chemistry Communications. 2021;131.

[22] Chu C, Qin Y, Ni C, Zou J. Halogenated benzothiadiazole-based conjugated polymers as efficient photocatalysts for dye degradation and oxidative coupling of benzylamines. Chinese Chemical Letters. 2022;33(5):2736-40.

[23] Fan Y, Ben H, Li L, Meng S, Zhang S, Zheng X, et al. A novel metal-free photocatalyst polyphenylene sulfide: Synthesis, characterization and performance evaluation. Applied Catalysis B: Environmental. 2020;274.

[24] AlHazmi GAA, AbouMelha KS, El-Desouky MG, El-Bindary AA. Effective adsorption of doxorubicin hydrochloride on zirconium metal-organic framework: Equilibrium, kinetic and thermodynamic studies. 2022;1258:132679.

[25] Gupta VK, Fakhri A, Azad M, Agarwal S. Synthesis and characterization of Ag doped ZnS quantum dots for enhanced photocatalysis of Strychnine asa poison: Charge transfer behavior study by electrochemical impedance and time-resolved photoluminescence spectroscopy. J Colloid Interface Sci. 2018;510:95-102.
[26] Huang K, Li C, Zheng Y, Wang L, Wang W, Meng X. Recent advances on silver-based photocatalysis: Photocorrosion inhibition, visible-light responsivity enhancement, and charges separation acceleration. Separation and Purification Technology. 2022;283.
[27] Irrgang N, Monneron-Enaud B, Möckel R, Schlömann M, Höck M. Economic feasibility of the co-production of indium from zinc sulphide using bioleaching extraction in Germany. Hydrometallurgy. 2021;200.
[28] Jegalakshmi E, Rameshbabu M, Razia M, Florence SS, Bakri M, Muthupandi S, et al. Structural, optical and antimicrobial activity of Ferric doped zinc sulphide (ZnS) nanoparticles. Materials Today: Proceedings. 2022;49:2611-4.
[29] Jiang L, Jia Z, Xu X, Chen Y, Peng W, Zhang J, et al. Preparation of antimicrobial activated carbon fiber by loading with silver nanoparticles. Colloids and Surfaces A: Physicochemical and Engineering Aspects. 2022;633.
[30] Hassan N, Shahat A, El-Didamony A, El-Desouky M, El-Bindary AA. Equilibrium, Kinetic and Thermodynamic studies of adsorption of cationic dyes from aqueous solution using ZIF-8. 2020. 2020;8(3):%J Moroccan Journal of Chemistry.
[31] Lange T, Reichenberger S, Ristig S, Rohe M, Strunk J, Barcikowski S, et al. Zinc sulfide for photocatalysis: White angel or black sheep? Progress in Materials Science. 2022;124.
[32] El-Bindary MA, El-Desouky MG, El-Bindary AA. Adsorption of industrial dye from aqueous solutions onto thermally treated green adsorbent: A complete batch system evaluation. Journal of Molecular Liquids. 2022;346:117082.
[33] Liu Y, Huang D, Cheng M, Liu Z, Lai C, Zhang C, et al. Metal sulfide/MOF-based composites as visible-light-driven photocatalysts for enhanced hydrogen production from water splitting. Coordination Chemistry Reviews. 2020;409.
[34] Lee WPC, Kong XY, Tan L-L, Gui MM, Sumathi S, Chai S-P. Molybdenum disulfide quantum dots decorated bismuth sulfide as a superior noble-metal-free photocatalyst for hydrogen evolution through harnessing a broad solar spectrum. Applied Catalysis B: Environmental. 2018;232:117-23.
[35] Li M, Zhong LX, Chen W, Huang Y, Chen Z, Xiao D, et al. Regulating the electron–hole separation to promote selective oxidation of biomass using ZnS@Bi2S3 nanosheet catalyst. Applied Catalysis B: Environmental. 2021;292.
[36] Maiti BK, Maia LB, Moura JJG. Sulfide and transition metals - A partnership for life. J Inorg Biochem. 2022;227:111687.
[37] Markovskaya DV, Gribov EN, Kozlova EA, Kozlov DV, Parmon VN. Modification of sulfide-based photocatalyst with zinc- and nickel-containing compounds: Correlation between photocatalytic activity and photoelectrochemical parameters. Renewable Energy. 2020;151:286-94.
[38] Miri A, Ghorbani F. Syntheses of Ag[Cu@Ag]\APTMS\boehmite as a photocatalyst for methylene blue degradation in batch and continuous flow systems under visible light. Environmental Nanotechnology, Monitoring & Management. 2021;16.
[39] Nilavazhagi A, Felixkala T. Adsorptive removal of Fe(II) ions from water using carbon derived from thermal/chemical treatment of agricultural waste biomass: Application in groundwater contamination. Chemosphere. 2021;282:131060.
[40] Gao X, Wang Z, Fu F, Li X, Li W. 2D double-layer-tube-shaped structure Bi2S3/ZnS heterojunction with enhanced photocatalytic activities. Physica B: Condensed Matter. 2015;474:81-9.
[41] Pham M-T, Hussain A, Bui D-P, Nguyen T-MT, You S-J, Wang Y-F. Surface plasmon resonance enhanced photocatalysis of Ag nanoparticles-decorated Bi2S3 nanorods for NO degradation. Environmental Technology & Innovation. 2021;23.
[42] Rafiq A, Ikram M, Ali S, Niaz F, Khan M, Khan Q, et al. Photocatalytic degradation of dyes using semiconductor photocatalysts to clean industrial water pollution. Journal of Industrial and Engineering Chemistry. 2021;97:111-28.
[43] Teo SH, Ng CH, Islam A, Abdulkareem-Alsultan G, Joseph CG, Janaun J, et al. Sustainable toxic dyes removal with advanced materials for clean water production: A comprehensive review. Journal of Cleaner Production. 2022;332.
[44] Tom AP. Nanotechnology for sustainable water treatment – A review. Materials Today: Proceedings. 2021.
[45] Trujillo-Rodriguez MJ, Anderson JL. Silver-based polymeric ionic liquid sorbent coatings for solid-phase microextraction: Materials for the selective extraction of unsaturated compounds. Anal Chim Acta. 2019;1047:52-61.
[46] Wu M, Chen H, Fan Y, Wang S, Hu Y, Liu J, et al. Carbonyl flavor compound-targeted colorimetric sensor array based on silver nitrate and o-phenylenediamine derivatives for the discrimination of Chinese Baijiu. Food Chem. 2022;372:131216.
[47] Sacco O, Vaiano V, Sannino D, Picca RA, Cioffi N. Ag modified ZnS for photocatalytic water pollutants degradation: Influence of metal loading and preparation method. J Colloid Interface Sci. 2019;537:671-81.
[48] Sakthivel R, Lin LY, Lee TH, Liu X, He JH, Chung RJ. Disposable and cost-effective label-free electrochemical immunosensor for prolactin based on bismuth sulfide nanorods with polypyrrole. Bioelectrochemistry. 2022;143:107948.
[49] Sharma K, Raizada P, Hasija V, Singh P, Bajpai A, Nguyen V-H, et al. ZnS-based quantum dots as photocatalysts for water purification. Journal of Water Process Engineering. 2021;43.
[50] Some S, Mondal R, Mitra D, Jain D, Verma D, Das S. Microbial pollution of water with special

reference to coliform bacteria and their nexus with environment. Energy Nexus. 2021;1.
[51] Subhiksha V, Kokilavani S, Sudheer Khan S. Recent advances in degradation of organic pollutant in aqueous solutions using bismuth based photocatalysts: A review. Chemosphere. 2022;290:133228.
[52] Xiong DN, Huang GF, Zhou BX, Yan Q, Pan AL, Huang WQ. Facile ion-exchange synthesis of mesoporous Bi2S3/ZnS nanoplate with high adsorption capability and photocatalytic activity. J Colloid Interface Sci. 2016;464:103-9.
[53] Yang H. A short review on heterojunction photocatalysts: Carrier transfer behavior and photocatalytic mechanisms. Materials Research Bulletin. 2021;142.
[54] Ye M, Shi F, Shen M, Qin W, Ren C, Yang Z. Composite soft-template method synthesis and biosensing application of hedgehog-like bismuth sulfide micro-nanostructures. Colloids and Surfaces A: Physicochemical and Engineering Aspects. 2021;613.
[55] You J, Liu C, Feng X, Lu B, Xia L, Zhuang X. In situ synthesis of ZnS nanoparticles onto cellulose/chitosan sponge for adsorption-photocatalytic removal of Congo red. Carbohydr Polym. 2022;288:119332.
[56] Ye Z, Kong L, Chen F, Chen Z, Lin Y, Liu C. A comparative study of photocatalytic activity of ZnS photocatalyst for degradation of various dyes. Optik. 2018;164:345-54.
[57] Zaitsev AV, Astapov IA. Prospects for creating regenerated photocatalytic materials for solar water treatment units. Materials Letters. 2022;310.
[58] Zhang H, Li H, Gao D, Yu H. Source identification of surface water pollution using multivariate statistics combined with physicochemical and socioeconomic parameters. Sci Total Environ. 2022;806(Pt 3):151274.
[59] Zhao G-q, Zheng Y-j, He Z-g, Lu Z-x, Wang L, Li C-f, et al. Synthesis of Bi2S3 microsphere and its efficient photocatalytic activity under visible-light irradiation. Transactions of Nonferrous Metals Society of China. 2018;28(10):2002-10.
[60] Zhou Z, Liu J, Zhou N, Zhang T, Zeng H. Does the "10-Point Water Plan" reduce the intensity of industrial water pollution? Quasi-experimental evidence from China. J Environ Manage. 2021;295:113048.